Dynamics of Relativistic Laser-Plasma Interaction on Solid Targets

Y. Ping,[1] A. J. Kemp,[1] L. Divol,[1] M. H. Key,[1] P. K. Patel,[1] K. U. Akli,[2] F. N. Beg,[3] S. Chawla,[3] C. D. Chen,[1] R. R. Freeman,[4] D. Hey,[1] D. P. Higginson,[3] L. C. Jarrott,[3] G. E. Kemp,[4] A. Link,[4] H. S. McLean,[1] H. Sawada,[3] R. B. Stephens,[2] D. Turnbull,[5] B. Westover,[3] and S. C. Wilks[1]

[1]*Lawrence Livermore National Laboratory, Livermore, California 94550, USA*
[2]*General Atomics, San Diego, California 92186, USA*
[3]*Department of Mechanical and Aerospace Engineering, University of California-San Diego, La Jolla, California 92093, USA*
[4]*College of Mathematical and Physical Sciences, Ohio State University, Columbus, Ohio 43210, USA*
[5]*Department of Mechanical and Aerospace Engineering, Princeton University, Princeton, New Jersey 08544, USA*

(Received 6 May 2011; published 5 October 2012)

A novel time-resolved diagnostic is used to record the critical surface motion during picosecond-scale relativistic laser interaction with a solid target. Single-shot measurements of the specular light show a redshift decreasing with time during the interaction, corresponding to a slowing-down of the hole boring process into overdense plasma. On-shot full characterization of the laser pulse enables simulations of the experiment without any free parameters. Two-dimensional particle-in-cell simulations yield redshifts that agree with the data, and support a simple explanation of the slowing-down of the critical surface based on momentum conservation between ions and *reflected* laser light.

DOI: 10.1103/PhysRevLett.109.145006 PACS numbers: 52.38.−r, 52.27.Ny

Relativistic laser-plasma interaction is of broad interest in modern physics, with applications ranging from particle acceleration [1], laboratory astrophysics [2], to fast ignition [3] for inertial confinement fusion [4]. During the interaction, the plasma conditions evolve rapidly upon intense laser irradiation, which modifies the partition of the deposited laser energy. Simulations have shown that the plasma density profile can be substantially steepened by the intense light pressure [5], which affects the energy spectrum of generated hot electrons [6] and their transport into the solid target [7]. Therefore time-resolved measurements are strongly desired to investigate the physical mechanisms and their consequences for various applications. However, among numerous studies of relativistic laser-plasma interaction, time-resolved measurements are quite scarce because the fast time scales (subpicosecond) and small spatial scales (micrometer) make these kinds of measurements very difficult.

Early time-resolved experiments on laser-plasma interaction at nonrelativistic intensities ($\sim 10^{17}$ W/cm^2) showed suppression of plasma expansion [8,9], and a transition from blue to red Doppler shift corresponding to the onset of hole boring [10]. Time-integrated data at 10^{18} W/cm^2 [11] and 10^{19} W/cm^2 [12] showed redshifts in the presence of preplasma, which can be explained by a simple model without taking into account the plasma thermal pressure [13]. In recent pump-probe experiments [14], Doppler spectrometry was used to study plasma motion up to 30 ps after the target was irradiated by a 30 fs laser at 5×10^{18} W/cm^2. As intensities reach above 10^{19} W/cm^2, however, the process can change dramatically. Previous experiments have shown that the total absorption of laser pulses is strongly enhanced in the relativistic regime [15]. As a result, the laser energy is deposited efficiently into the target, with substantial energy taken by energetic electrons. To study this effect on hole boring we have developed a novel time-resolved diagnostic based on frequency-resolved optical gating (FROG) [16] to measure the time history of the interaction in the relativistic regime [17]. Using this technique the frequency shift of specular light is measured in a single shot with a time resolution of ~100 fs. We observed for the first time a continuously decreasing redshift that occurs even when the laser intensity is increasing. Particle-in-cell (PIC) simulations have been performed using measured laser parameters and the results agree well with the time-resolved data.

The experiment was performed on the Titan laser in the Jupiter laser facility at Lawrence Livermore National Laboratory. Titan is a Nd:glass laser system delivering 150 J, 1053 nm laser pulses as short as 0.7 ps at full width of half maximum (FWHM), or up to 300 J for 10 ps pulses. The experimental setup is illustrated in Fig. 1(a). The targets were simple 1 mm-thick slabs with aluminum as the front layer. The laser pulse was focused by an $f/3$ off-axis parabola onto the target at an incident angle of 16°. The full characteristics of incident laser pulses were measured with a suite of on-shot laser diagnostics, including a FROG for the laser temporal shape and phase, a water cell for prepulses, and an equivalent plane monitor for the focal spot [18].

The light in the specular direction was collected by an $f/10$ lens and collimated by a telescope before entering another FROG (specular FROG) operating near 527 nm with a polarization gating scheme [16]. An edge filter was inserted to reject the 1ω light. We chose 2ω because it was

generated mainly at critical density while 1ω can be scattered at a range of densities [19]. Since beam uniformity is important for reliable FROG measurements, cylindrical lenses were used to create a line focus onto the nonlinear glass, which not only minimized the nonuniformity in the spatial profile but also enhanced the sensitivity of this diagnostic. The 2D FROG trace was recorded by a charge-coupled device camera. The line focus was imaged into another charge-coupled device camera to check the uniformity for every shot. The variation of intensity along the line focus was found to be within $\pm 10\%$, hence confirming the validity of the FROG data.

A typical FROG trace is displayed in Fig. 1(b). This shot was taken for a quasi-Gaussian incident laser pulse with FWHM of 1.4 ps and a total energy of 150 J. The prepulse was measured to be 17 mJ lasting 3 ns preceding the main pulse. The measured vacuum focal spot indicated an intensity of 5×10^{19} W/cm^2 at the 20th percentile and 1.5×10^{19} W/cm^2 at the 50th percentile. The FROG traces were analyzed using FEMTOSOFT® software to retrieve the phase as a function of time [16]. The instantaneous frequency was obtained as the time derivative of the phase. The relative spectral shift, $\Delta\lambda/\lambda_0$ ($\lambda_0 = 526.5$ nm), is plotted in Fig. 2 (black line). The plot was averaged over 5 shots to reduce the noise level. The error bars include uncertainties in calibration, phase retrieving, and shot-to-shot fluctuations. The data show that the redshift was largest at the beginning, reaching $\sim 6\%$. The redshift gradually decreases over time, dropping to zero at ~ 3 ps and ending as a 1.5% blueshift. The spectral shift can be attributed to three processes: relativistic self-phase-modulation [20], Doppler shift due to relativistic effect, and Doppler shift due to density steepening or expansion. The first effect was estimated using the preplasma density profile calculated by a 2D radiation-hydrodynamic simulation with the code HYDRA [21] and the measured prepulse. It is at least $3\times$ smaller than the observed shift, and steepening of the density profile makes the self-phase-modulation even less. The second effect is due to modification of the critical density, $\gamma(t)n_c$, where n_c is the nonrelativistic critical density, and γ is the relativistic factor, $\gamma = \sqrt{1 + a_0^2/2}$ for linearly polarized light with amplitude a_0 [13]. The effective motion of n_c location due to varying intensity was estimated using the HYDRA preplasma profile, and it turns out to be negligible compared to the observed shift. Therefore, the dominant contribution to the measured shift should be density steepening or expansion. The 6% redshift at the beginning corresponds to a receding velocity of 0.03 c, where c is the speed of light. The transition to a blueshift over time indicates reversal of the surface motion from inward ponderomotive pushing to outward expansion.

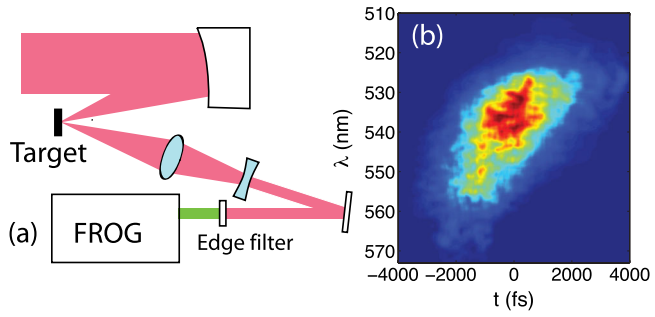

FIG. 1 (color online). (a) Setup for FROG measurements of specular light. (b) A typical specular FROG trace.

Two-dimensional PIC simulations of the laser plasma interaction were performed with the code PSC [22]. Care has been taken to implement the experimental conditions in the simulation setup. The preplasma density profile and effective ion charge states were provided by HYDRA simulations with the measured prepulse. While the ion charge states in the preplasma are determined self-consistently by HYDRA, ionization during the main pulse interaction was ignored because the aluminum preplasma is already $>90\%$ ionized. The initial expanding velocity of the preplasma was also ignored since the corresponding $\Delta\lambda/\lambda_0$ is $\sim 0.1\%$. The near-field intensity distribution of the incident laser pulse was reconstructed by matching the power spectrum of the generated focus with that of the measured high-power focal spot. This near field was used as a boundary condition for the Maxwell solver in the PIC simulation. The simulation box extended over 180 μm $\times$ 150 μm, resolved with 32 cells per laser wavelength and 74 steps per laser cycle, with 50 electrons and ions per cell. Electron density was capped at $100n_c$ to reduce numerical heating effects, and the underdense region was terminated at $0.04n_c$ for computational efficiency. Boundary conditions were periodic in the transverse direction and absorbing in the longitudinal direction. The critical density surface was located 100 μm from the laser injection plane to allow for enough underdense and vacuum regions. The temporal

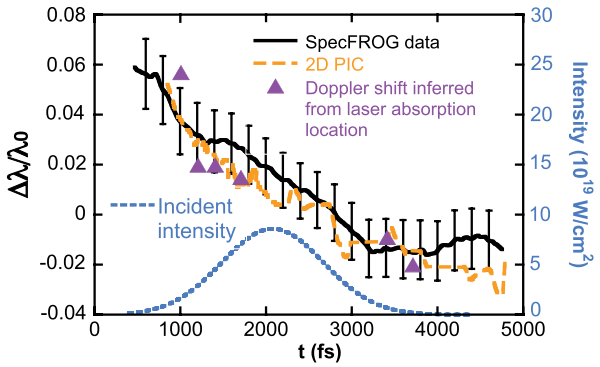

FIG. 2 (color online). Comparison of measured and simulated time history of spectral shift. Black solid line: specular FROG data. Orange dashed line: central wavelength of specular 2ω spectrum in the 2D PIC run. Purple triangles: expected Doppler shift inferred from motion of laser absorption point in the 2D PIC run. Blue dashed line: incident vacuum peak intensity (99th percentile).

shape of the incident laser pulse was Gaussian with a FWHM of 1.4 ps, beginning at e^{-4} of the peak power. Including the low-intensity front was found to be important to reproduce the history of the reflected light. The fraction of specular light around $2\omega_0$, integrated over 5 ps, is consistent with calorimeter data in place of FROG in the experiment.

The simulation allowed us to determine the location where the wavelength shift occurs in the specular light by tracking the 2ω signal at various distances from the target. The result confirms the localization of 2ω generation and frequency shift near $n_e = \gamma n_c$. To compare with the data, the backward-propagating electromagnetic wave was recorded at the boundary in the specular direction and a fast Fourier transform was carried out for each 200 fs segment of the time series to obtain time history of the spectra, leading to a resolution of 0.75% in frequency space. For each segment, a central wavelength was determined by a Gaussian fit of the spectrum. The spectral shift vs time from the simulations is plotted in Fig. 2 (orange dashed line), which is in good agreement with the experimental data (the time axis was aligned to overlap the peak of 2ω intensity with data). The expected Doppler shift deduced from the motion of the laser absorption or reflection point in the simulation, also shown in Fig. 2(a) (purple triangles), agrees well with the measured and simulated shift, confirming that the observed shift is dominated by the Doppler effect caused by density steepening or expansion. The quantitative agreement between the data and the simulation is not accidental as the shift depends on both the preplasma profile and the reflected laser intensity as explained by a model presented below. Agreement is obtained only when the experimental conditions are properly implemented in the simulations.

Figure 3(a) displays a 2D spatial map of the laser Poynting flux and electron density at the peak of the laser power in the PIC simulation. Clearly filamentation occurs and the location of the critical density has receded by 6 μm. Shown in Fig. 3(b) is the time history of incident peak laser intensity at the 99th percentile (blue dashed line) and actual peak intensity on target (red solid line). The latter is higher than the former by $\sim 2\times$ for most of the time, indicating that filamentation occurs fairly early in time. The inset in Fig. 3(a) displays an image of a typical Titan focus taken on shot in this experiment. The focus was highly elongated with an aspect ratio of 4:1 along the 50% contour. This quasiline focus makes the 2D simulation a good approximation for the experiment. In order to examine the filamentation in three dimensions, we performed a reduced-scale 3D PIC simulation with the measured focus (a full-scale 3D run is computationally too expensive). It turns out that the filamentation in three dimensions resembles the 2D case, including the factor of 2 between the on-target intensity and the vacuum intensity, which is important for predicting the correct "push" by the light on the plasma near the main filament. As a side note, if

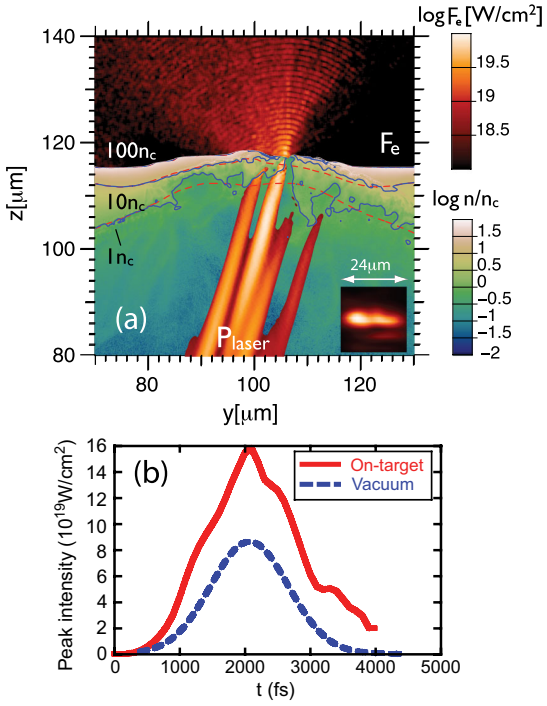

FIG. 3 (color online). (a) Snapshot of laser Poynting flux (P_{laser}), electron density (contour lines), and electron energy flux (F_e) at peak power in the 2D PIC simulation. The red dashed contour lines are at $t = 0$ and the blue lines are at $t = 2.2$ ps. The inset is a typical on-shot Titan vacuum focus. (b) Time history of incident peak intensity (blue dashed line) and actual peak intensity on target (red solid line).

the focus were transform limited, $2\times$ enhancement of intensity in two dimensions would correspond to $4\times$ enhancement in three dimensions. However, the actual laser spot is far from ideal, and the elongated focus leads to 2D-like behavior.

After demonstrating agreement between the experiment and our two-dimensional simulation, we aim to understand the physics effects that cause the slowing-down of the critical interface in a simplified quasi-one-dimensional approach.

We start by writing energy and momentum flux balance between laser and plasma components as

$$I_+/c + I_-/c = P_e + P_i, \tag{1}$$

$$I_+ - I_- = F_e + F_i, \tag{2}$$

where $I_{+/-}$ denotes incident and reflected intensity, $P_{e/i}$ is momentum, and $F_{e/i}$ is the energy flux density of electrons or ions, respectively. Due to symmetry around the laser axis, lateral energy and momentum fluxes cancel out so that we can focus on the forward-going components. In our case, the electrons' momentum and energy distributions peak at relativistic energies where $\gamma \gg 1$ and $\beta \approx c$ so that $F_e \approx cP_e$, while the ion energy flux is negligible. Therefore, the momentum transferred to plasma ions is

$$P_i \simeq 2I_-/c. \quad (3)$$

In other words, ion momentum is gained from elastically backscattered light. In the limit of 100% reflectivity, our model is in agreement with previous work [13]. In the other limit of 100% absorption, all the momentum is taken by energetic electrons. In situations where absorption is high as in the relativistic regime, hole boring will be much less than expected from the previously used expression $P_i = (I_+ + I_-)/c$ [12,15,23,24].

For the purpose of verifying our new expression for P_i and to identify the cause of the apparent slowing-down of the absorption point during the *rise* in laser intensity, we have performed a reduced 2D simulation with a transverse size of four laser wavelengths and uniform laser irradiation. This simulation shares the high absorption found in our 2D simulation as well as the slowing-down of the critical interface.

With Eq. (3) for P_i in hand, we apply a simple momentum-flux conservation model [13] to track the motion of the absorption point $z_a(t)$ in the reduced 2D simulation. This model indicates that the momentum transfer to ions is

$$P_i(t) = 2u^2(t)n_i(z_a)M_i, \quad (4)$$

where n_i is the *initial* ion density profile because the laser-accelerated ions move into the bulk target at a higher speed than the absorption point so they do not contribute to the momentum flux balance at the laser-plasma interface.

Figure 4(a) compares the motion of the absorption point in the reduced simulation, determined as the point where the electromagnetic field vanishes, to that obtained by integrating Eq. (4) starting at 1 ps. Before that time the laser amplitude $a_0 \approx 1$ so that the light filaments in near-critical density plasma, which makes it difficult to define the absorption point. Fig. 4(b) presents the momentum transfer between reflected laser light and the plasma. Our expression for the ion momentum flux P_i, as well as overall momentum and energy conservation in our reduced 2D simulation hold to good precision. A comparable 1D simulation also agrees with Eq. (3), but yields about 2.5× lower absorption than the reduced 2D case.

The motion predicted by our simple model matches the one observed in the reduced-2D simulation up to the peak power, as shown in Fig. 4(a), indicating that the slowing-down of the critical surface motion can be explained by the exponential increase in density of the preformed plasma. This means that the reflected photon momentum is transferred to ions at the absorption interface in a collisionless process (via the electrons, through electrostatic fields). Note that the scale length of the preformed plasma is such that the laser pulse never interacts with more than $\sim 30 n_c$ electron density, which is, in the context of this experiment, practically free of collisional effects at temperatures above 1 keV [25–28]. This is why our simulations give almost identical results with and without collisions. The isotropic component of the bulk electron

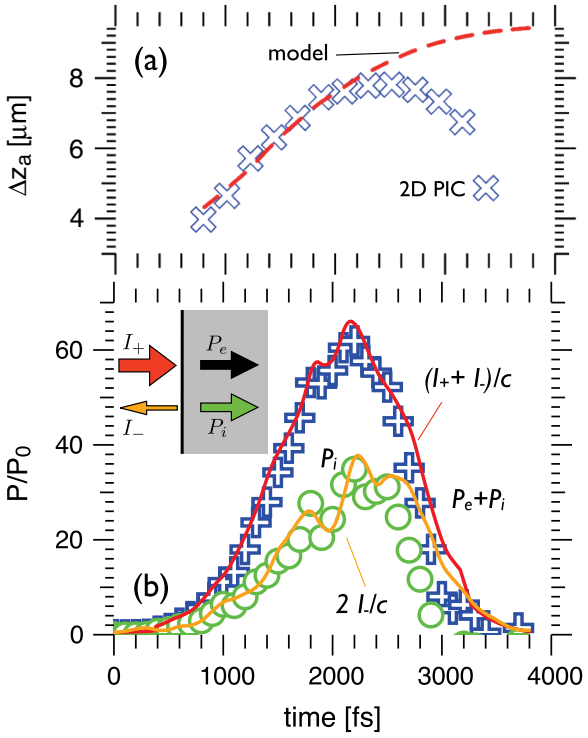

FIG. 4 (color online). (a) Motion of the laser absorption point in reduced 2D PIC simulation vs simple model. The symbols are the locations where the laser field vanishes (uncertainties due to 2D structure are represented by the finite size). The line represents the motion predicted by Eq. (4). All positions are relative to the point where $n_e(0) = n_c$. (b) Momentum flux balance between laser light and plasma in units of $P_0 \equiv n_c m_e c^2 \approx 1$ Gbar for 1 μm wavelength light. The lines represent the laser momentum, and the symbols represent the electron or ion momentum.

pressure tensor (thermal pressure, P_{th}) behind the interaction interface, estimated as the product of the local density and temperatures corresponding to fits to relativistic Maxwell-Juttner distribution functions, is less than the directional component of the pressure tensor covered by Eq. (4) up to the peak power. The compression work performed by the laser to the plasma in an area A for a time interval dt, expressed as $PdV = P_{\text{th}} v A dt$, is negligible compared to the irradiated laser power since the velocity of the motion $v \ll c$. After the peak of the laser power, the thermal pressure takes over and the plasma expands, causing a blueshift of the reflected light. The plasma response at this stage beginning at 2.2 ps is not covered by the simple momentum flux conservation model in Eqs. (3) and (4). A realistic description of the expansion needs to be at least two-dimensional and include heat loss mechanisms such as nonlocal heat conduction and radiation; on top of that, more precise measurements would be required for any quantitative comparison with modeling, which is beyond the scope of this Letter.

To summarize, time-resolved Doppler shift measurements during laser-plasma interaction show slowing-down

of the hole boring at intensities up to $\sim 10^{20}$ W/cm^2 in front of solid targets. A momentum conservation model indicates that the hole boring velocity is determined by the reflected light rather than incident light. The sustained high absorption of laser light in the relativistic regime results in little momentum transfer to the plasma, and the motion of the critical surface is slowed down by exponential increase of the preplasma density profile. Our 2D PIC simulations agree well with the time-resolved data and support this interpretation. The sensitivity of the Doppler shift to the plasma profile and *in situ* laser intensity renders the specular FROG as a useful single-shot probe for relativistic laser-plasma interaction with access to densities $n > n_c$.

We wish to thank the Jupiter laser facility team at LLNL for laser operation and technical support. This work was performed under the auspices of U.S. Department of Energy by LLNL under Contract No. DEAC52-07NA27344. Computational effort for this work was supported by the LLNL Institutional Computing Grand Challenge program.

[1] S. P. D. Mangles *et al.*, Nature (London) **431**, 535 (2004); C. G. R. Geddes, Cs. Toth, J. van Tilborg, E. Esarey, C. B. Schroeder, D. Bruhwiler, C. Nieter, J. Cary, and W. P. Leemans, Nature (London) **431**, 538 (2004); J. Faure, Y. Glinec, A. Pukhov, S. Kiselev, S. Gordienko, E. Lefebvre, J.-P. Rousseau, F. Burgy, and V. Malka, Nature (London) **431**, 541 (2004).

[2] B. A. Remington, D. Arnett, R. P. Drake, and H. Takabe, Science **284**, 1488 (1999).

[3] M. Tabak, J. Hammer, M. E. Glinsky, W. L. Kruer, S. C. Wilks, J. Woodworth E. M. Campbell, M. D. Perry, and R. J. Mason, Phys. Plasmas **1**, 1626 (1994); R. Kodama *et al.*, Nature (London) **418**, 933 (2002).

[4] M. H. Key, R. G. Evans, Nature (London) **313**, 94 (1985); T. Ditmire, J. Zweiback, V. P. Yanovsky, T. E. Cowan, G. Hays, and K. B. Wharton, Nature (London) **398**, 489 (1999).

[5] A. J. Kemp, Y. Sentoku, and M. Tabak, Phys. Rev. Lett. **101**, 075004 (2008).

[6] B. Chrisman, Y. Sentoku, and A. J. Kemp, Phys. Plasmas **15**, 056309 (2008).

[7] A. G. MacPhee *et al.*, Phys. Rev. Lett. **104**, 055002 (2010).

[8] X. Liu and D. Umstadter, Phys. Rev. Lett. **69**, 1935 (1992).

[9] P. Audebert, J. P. Geindre, S. Rebibo, and J. C. Gauthier, Phys. Rev. E **64**, 056412 (2001); S. Rebibo, J.-P. Geindre, P. Audebert, G. Grillon, J.-P. Chambaret, and J.-C. Gauthier, Laser Part. Beams **19**, 67 (2001).

[10] R. Kodama, K. Takahashi, K. A. Tanaka, M. Tsukamoto, H. Hashimoto, Y. Kato, and K. Mima, Phys. Rev. Lett. **77**, 4906 (1996).

[11] M. P. Kalashnikov, P. V. Nickles, T. Schlegel, M. Schnuerer, F. Billhardt, I. Will, and W. Sandner, Phys. Rev. Lett. **73**, 260 (1994).

[12] M. Zepf *et al.*, Phys. Plasmas **3**, 3242 (1996).

[13] S. C. Wilks, W. L. Kruer, M. Tabak, and A. B. Langdon, Phys. Rev. Lett. **69**, 1383 (1992).

[14] S. Mondal, A. D. Lad, S. Ahmed, V. Narayanan, J. Pasley, P. P. Rajeev, A. P. L. Robinson, and G. R. Kumar, Phys. Rev. Lett. **105**, 105002 (2010).

[15] Y. Ping *et al.*, Phys. Rev. Lett. **100**, 085004 (2008).

[16] R. Trebino, *Frequency-Resolved Optical Gating: The Measurements of Ultrashort Laser Pulses* (Kluwer, Boston, 2000).

[17] R. J. Kingham, P. Gibbon, W. Theobald, L. Veisz, and R. Sauerbrey, Phys. Rev. Lett. **86**, 810 (2001).

[18] A. G. MacPhee *et al.*, Rev. Sci. Instrum. **79**, 10F302 (2008).

[19] A. Tarasevitch, K. Lobov, C. Wunsche, and D. von der Linde, Phys. Rev. Lett. **98**, 103902 (2007).

[20] I. Watts, M. Zepf, E. L. Clark, M. Tatarakis, K. Krushelnick, A. E. Dangor, R. Allott, R. J. Clarke, D. Neely, and P. A. Norreys, Phys. Rev. E **66**, 036409 (2002).

[21] M. Marinak, S. W. Haan, T. R. Dittrich, R. E. Tipton, and G. B. Zimmerman, Phys. Plasmas **5**, 1125 (1998).

[22] B. I. Cohen, A. J. Kemp, and L. Divol, J. Comput. Phys. **229**, 4591 (2010).

[23] Y. Sentoku, W. Kruer, M. Matsuoka, and A. Pukhov, Fusion Sci. Technol. **49**, 278 (2006).

[24] P. Gibbon, *Short-pulse Laser Interactions with Matter* (Imperial College, London, 2007), p. 187.

[25] W. Theobald *et al.*, Phys. Plasmas **13**, 043102 (2006).

[26] R. G. Evans *et al.*, Appl. Phys. Lett. **86**, 191505 (2005).

[27] K. U. Akli *et al.*, Phys. Rev. Lett. **100**, 165002 (2008).

[28] P. M. Nilson *et al.*, Phys. Plasmas **18**, 056703 (2011).